Applied Catalysis A: General 349 (2008) 76–85

Contents lists available at ScienceDirect

Applied Catalysis A: General

journal homepage: www.elsevier.com/locate/apcata

Product selectivity and catalytic deactivation of MOR zeolites with different acid site densities in methanol-to-olefin (MTO) reactions

Ji Won Park [a], Sun Jung Kim [a], Myungeun Seo [b], Sang Youl Kim [b], Yoshihiro Sugi [c], Gon Seo [a,*]

[a] School of Applied Chemical Engineering and the Center for Functional Nano Fine Chemicals, Chonnam National University, Gwangju 500-757, Republic of Korea
[b] Department of Chemistry, KAIST, 335 Gwahagno (373-1 Guseong-dong), Yuseong-gu, Daejeon, Republic of Korea
[c] Department of Materials Science and Technology, Faculty of Engineering, Gifu University, Gifu 501-1193, Japan

ARTICLE INFO

Article history:
Received 15 April 2008
Received in revised form 10 July 2008
Accepted 14 July 2008
Available online 19 July 2008

Keywords:
Methanol to olefin (MTO)
MOR zeolite
Acid site density
Deactivation

ABSTRACT

The effects of the acid site densities of MOR zeolites on their product selectivity and deactivation were investigated in the methanol-to-olefin (MTO) reactions. The MOR zeolites showed a high conversion and high yield of the lower olefins at the initial time of the MTO reaction, regardless of their acid site density. However, the conversion and the yield of the lower olefins over them rapidly decreased in the order of MOR(103) < MOR(55) < MOR(12) < MOR(5), where the numbers in parenthesis represent their Si/Al ratios. The materials occluded on the MOR zeolites during the MTO reaction were investigated by the IR, ^{13}C NMR and UV–vis spectroscopic methods. A large amount of polycyclic aromatic hydrocarbons (PAHs) with 3–4 fused aromatic rings was occluded on the MOR(5) zeolite with the highest acid site density. However, alkylbenzenes and alkylnaphthalenes were the major components of the materials occluded on the MOR(103) zeolite with the lowest acid site density. The IR spectra recorded *in situ* during the MTO reaction over the MOR zeolites clearly exhibited the differences in the accumulation rates of PAH on their pores according to the acid site density. The rapid accumulation of PAH on the MOR zeolites with high acid site densities leads to the loss of the active alkylbenzene intermediates as well as to the blockage of the pores, resulting in their rapid deactivation. The sparse distribution of acid sites in the pores of the MOR zeolites suppresses the condensation of alkylbenzenes in their pores and lengthens their catalyst lifetime.

1. Introduction

Low olefins such as ethylene, propylene and butenes have been used as raw materials of polyolefins and as the starting materials for various chemicals in the petrochemical industry. Although the thermal cracking of naphtha is still a major process for the production of lower olefins, the thermal cracking of ethane and the fluidized catalytic cracking of middle distillates have become important as supplementary production processes of the lower olefins. Furthermore, the rapid increase in the price of crude oil lowers the feasibility of the thermal cracking of naphtha, because of the latter's high price. The high-temperature operation of the thermal cracking process inevitably requires a large amount of energy and causes a large amount of carbon dioxide to be emitted. As a result, alternative processes for the production of lower olefins from non-petroleum sources without using a large amount of energy have been steadily studied [1–3].

The production of lower olefins using the methanol-to-olefin (MTO) process has been considered to be a plausible alternative since methanol can be manufactured from various sources such as coal, natural gas and biomass. The control of the product distribution in the MTO reaction by varying the catalysts and reaction conditions also provides a powerful way to produce a given olefin selectively. Especially, the high selectivity for propylene over a SAPO-34 molecular sieve in the MTO reaction is very useful to meet the steady increase in demand for propylene [2].

Methanol is converted to lower olefins over zeolite catalysts through dimethyl ether [1,3–5]. Since the lower olefins react with each other on the acid sites and produce paraffins and aromatics, their further reactions have to be suppressed in order to enhance the selectivity for the lower olefins. Actually, the partial neutralization of the strong acid sites of zeolites by impregnating them with phosphorous compounds significantly improves the selectivity for the lower olefins in the MTO reaction [3]. Using zeolites with small micropores is also effective in enhancing the selectivity for the lower olefins, by limiting the transfer of *iso*-hydrocarbons and aromatics due to their molecular sizes [4–6]. A SAPO-34 molecular sieve with

* Corresponding author. Tel.: +82 62 530 1876; fax: +82 62 530 1899.
E-mail address: gseo@chonnam.ac.kr (G. Seo).

0926-860X/$ – see front matter © 2008 Elsevier B.V. All rights reserved.
doi:10.1016/j.apcata.2008.07.006

pore entrances consisting of 8 membered rings (8MR) shows high selectivity for the lower olefins, because of its small pore entrances [4]. The UOP/Hydro MTO process employs a Ni/SAPO-34 molecular sieve as a catalyst and achieves a high yield of the lower olefins of more than 85% [2,5]. The ERI, LTA and UFI zeolites with 8MR pore entrances also show high selectivity for the lower olefins in the MTO reaction, due to the limitations in the size of their pore entrances in the fresh state, but they rapidly become deactivated due to the accumulation of PAHs in their cages [6].

MOR and BEA zeolites with 12MR pore entrances, therefore, are not effective as industrial catalysts in the MTO reaction, because of their low selectivity for the lower olefins and rapid deactivation. However, the MOR zeolite with a lower acid site density, prepared by careful removal of aluminum atoms from its framework, shows slow deactivation and high selectivity for the lower olefins [7–11]. Although the careful dealumination of the MOR zeolite to reduce its acid site density without destroying its pore structure is suggested to maintain its activity in the MTO reaction, the catalytic role of the acid site density in its deactivation was not discussed. Moreover, the reaction path of the MTO reaction and the selectivity for the lower olefins over large pore zeolites have not been systematically studied [7,10].

Many active species such as carbenes, free radicals, alkoxy ions and oxonium ions have been suggested as intermediates in the MTO reaction to explain its reaction mechanism and product distribution over zeolite catalysts [12]. However, the *in situ* NMR study on the MTO reaction over SAPO-34 molecular sieve suggested the hydrocarbon pool mechanism in which multimethylbenzenes are formed in the cages of SAPO-34 and act as active intermediates [13–17]. Hexamethylbenzene (HMB) molecules located in the cages react with methanol and produce the lower olefins through paring and side-chain alkylation reactions [14,15]. The formation of HMB requires an induction time for the generation of active intermediates, and the condensation of HMB to PAH causes the deactivation of the SAPO-34 catalyst [6,16,17]. Therefore, it may be reasonable to conclude that the lowering of the acid site density of MOR zeolites reduces the concentration of HMB in their pores and suppresses the condensation of the HMB molecules themselves. If the MTO reaction proceeds over MOR zeolites through the hydrocarbon pool mechanism, as in the case of SAPO-34, despite their different pore sizes, MOR zeolites with a low acid site density and uniform pores would be expected to show high catalytic performance in the MTO reaction, as well as high selectivity for the lower olefins.

In this study, we investigate the MTO reactions over four MOR zeolites with different Si/Al ratios to clarify the effect of the acid site density on their product selectivity and catalyst deactivation behaviors. The large one-dimensional pores and the strong framework structure of the MOR zeolites eliminate the other possible contributions of the pore structures and sizes to the MTO reaction. The occlusion of materials in the pores of the MOR zeolites was examined using various spectroscopic methods to reveal the reactions which take place there during the MTO reaction.

2. Experimental

2.1. Characterization of catalysts

MOR zeolites with Si/Al ratios of 5, 12, 55 and 103 were employed as catalysts in the MTO reaction. These zeolites were purchased from Tosoh Corporation and were known to be prepared through the dealumination of the parent MOR zeolite [18,19]. The MOR zeolites were classified by indicating their Si/Al ratios in parentheses after the MOR code name.

The XRD patterns of the MOR zeolites were recorded on a high-resolution X-ray diffractometer (HR-XRD, Rigaku D/MAX Ultima III) at 40 kV and 40 mA. Ni-filtered Cu Kα X-ray radiation (λ = 1.54056 Å) was employed. The shape and the size of the MOR zeolites were examined by a scanning electron microscope (SEM, Hitachi, S-4700).

The adsorption isotherms of nitrogen on the MOR zeolites were obtained using an automatic volumetric adsorption apparatus (Mirae SI, NanoPorosity-XQ). The MOR zeolites were evacuated at 250 °C for 2 h prior to exposing them to nitrogen gas. Their surface areas were calculated using the BET equation and the volumes of the micropores and mesopores were determined using the *t*-plot and the BJH method, respectively.

The temperature programmed desorption (TPD) profiles of ammonia from the MOR zeolites were recorded on a homemade TPD apparatus. 0.1 g of the MOR zeolite was charged in the center of a quartz reactor (o.d. = 1/4 in.) and pretreated in a helium (Shinil, 99.999%) flow of 100 ml min^{-1} at 500 °C for 2 h. After being cooled to 150 °C, the zeolite sample was saturated by adding pulses of ammonia (Koreagas, 99.999%). The physically adsorbed ammonia was removed by purging the zeolite sample with the helium flow for 1 h. The temperature of the reactor was then increased to 600 °C at a ramping rate of 10 °C min^{-1}. The desorption of ammonia from the zeolite sample was continuously monitored by a mass spectrometer (Balzers, QMS 200).

2.2. MTO reaction

The MTO reaction over the MOR zeolites was carried out in an atmospheric flow reactor system described in our previous paper [20]. 0.1 g of the catalyst charged in the center of a quartz reactor (o.d. = 1/2 in.) was activated at 550 °C in a nitrogen (Shinil, 99.999%) flow of 120 ml min^{-1} for 2 h. Methanol vapor ($^{12}CH_3OH$, Duksan, 99%) diluted in a nitrogen flow of 30 ml min^{-1} was fed to the catalyst at 350 °C. The feed rate of methanol was adjusted to 0.087 ml h^{-1} (WHSV = 0.70 h^{-1}) by setting the temperature of the methanol evaporator installed in the circulator (JEIO TECH, RBC-100).

The products of the MTO reaction were analyzed using a gas chromatograph (D.S. Science, DS 6200) equipped with a CP-Volamine capillary column and an FID detector. The product samples captured in a multiposition sampling valve (Valco) were sequentially injected to ensure sufficient analyzing times. The temperature of the column was maintained at 50 °C for 5 min and then increased to 240 °C at a ramping rate of 10 °C min^{-1}. Since anthracene was detected starting from 52 min after the injection of the product pulse, the total analyzing time for each run was set to 1 h.

The conversion of methanol was defined as the percentage of methanol consumed in the MTO reaction and the yield of a given product was defined as the percentage of methanol consumed for its production. The yield of the lower olefins was defined as the sum of the yields of ethylene, propylene and butenes.

2.3. Characterization of occluded materials on MOR zeolites

The occlusion of hydrocarbons on the MOR zeolites in the MTO reaction was investigated by means of an FT-IR spectrophotometer (BIO-RAD, FTS-175C) equipped with an *in situ* cell (GRASEBY SPECAC). A 10 mg zeolite wafer was supported on a sample holder and activated at 500 °C in a nitrogen flow of 100 ml min^{-1} for 1 h. Methanol was injected in a nitrogen flow of 30 ml min^{-1} using a syringe pump (Sinmyung, KdSeries 100) at 350 °C for the MTO reaction. The feed rate of methanol was adjusted to 0.20 μl min^{-1} to obtain the same space velocity as that in the MTO reaction

carried out in the flow reactor. The differential IR spectra were recorded in *in situ* mode during the MTO reaction in the wavenumber range of 4000–700 cm^{-1} with a resolution of 4 cm^{-1}. Tetradeutromethanol (CD_3OD, Aldrich, D 99.8%) was also used as a reactant to clearly assign the IR absorption bands of the materials occluded on the MOR zeolites. In addition, 1-methylnaphthalene (MNP) and 1,3,5-trimethylbenzene (TMB) were also used as a reference materials to clearly assigned IR adsorbed on the MOR(12) zeolite at 120 °C. The feed rate of MNP and TMB was adjusted to 0.10 μl min^{-1} carried out in the flow reactor.

The ^{13}C NMR spectra of the materials occluded on the MOR zeolites in the MTO reaction were obtained using a ^{13}C MAS NMR spectrometer (Varian, Unity Solid Inova WB 200 MHz System). Methanol enriched with ^{13}C ($^{13}CH_3OH$, ^{13}C 99%, Aldrich) was fed to the sample of MOR zeolites charged in the flow reactor at 350 °C for 90 min. The low boiling materials remaining in the catalyst were removed by purging with nitrogen flow immediately after the methanol feed was stopped. The used catalyst was transferred to an NMR sample rotor in a glove box. The resonance frequency of ^{13}C was 50.657 MHz and its $\pi/2$ rad pulse width was 3 μs with a 10 s recycle delay. The magic angle spinning rate was 5 kHz. 2000 scans were accumulated to enhance the signal-to-noise of the NMR spectra.

The amount of materials occluded on the MOR zeolites during the MTO reaction was measured using a thermogravimetric analyzer (TG/DTA-200, Seiko Inc.). The change in the mass of the used catalysts was recorded with increasing temperature from 25 to 800 °C in air.

The MOR zeolites used in the MTO reaction at 350 °C for 6 h were dissolved using hydrofluoric acid (J.T. Baker, 48%). The dissolved phase was neutralized with potassium carbonate (Osaka Hayashi, 99.5%). The organic materials occluded on the zeolites were extracted with carbon tetrachloride (Duksan, 95%) [21]. The water contained in the extracts was removed using sodium sulfate (Duksan, 99%). The UV–vis spectra of the extracts were recorded on a UV–vis spectrophotometer (Ocean Optics Inc., USB 2000).

3. Results

3.1. Physicochemical properties of the MOR zeolites

Since the Si/Al ratio of the parent MOR zeolite synthesized from its aqueous synthetic mixture is 5, the MOR zeolites with higher Si/Al ratios are usually prepared by treating the parent MOR zeolite with acid solutions to remove aluminum atoms from its framework [10]. The framework of the MOR zeolites is quite stable against acid; thus, their pore structure would be expected to be retained after the dealumination. Fig. 1 shows the XRD patterns of the MOR zeolites employed in this study. Their Si/Al ratios vary from 5 to 103, but their XRD patterns are in good coincidence with the pattern reported in the literature [22,23]. The characteristic diffraction peaks of the MOR zeolites with higher Si/Al ratios are slightly higher than those of the parent MOR zeolite, even though they were prepared by the acid treatment. The partial removal of the amorphous materials contained in the parent MOR zeolite may be the cause of the increase in the diffraction peaks of the MOR zeolites with higher Si/Al ratios.

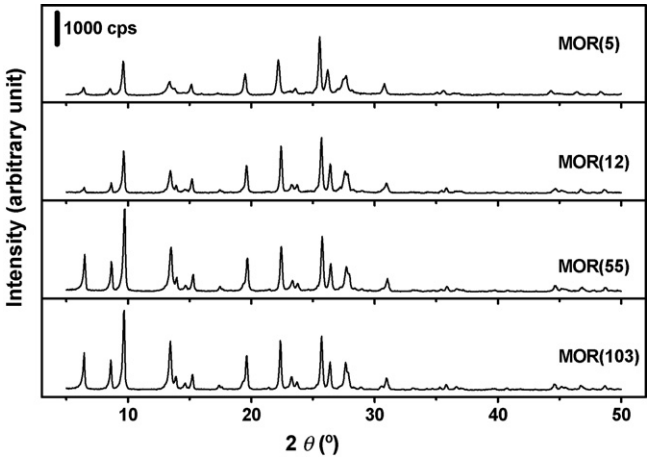

Fig. 1. X-ray diffraction patterns of the MOR zeolites.

The MOR zeolites are composed of bundled needle-type crystallites, as shown in Fig. 2. The difference in the size of the MOR zeolites according to their Si/Al ratios is not remarkable.

Fig. 3 shows the adsorption isotherms of nitrogen on the MOR zeolites. The isotherm on the MOR(5) zeolite is a typical Langmuir one, while those on the MOR zeolites with higher Si/Al ratios show gradual increases in the amount of nitrogen adsorbed with increasing pressure of nitrogen. The removal of the amorphous materials during the acid treatment induces the formation of micropores and mesopores, resulting in a small increase in the amount of nitrogen adsorbed. These increases in the nitrogen adsorption on the MOR zeolites with higher Si/Al ratios result in a gradual increase in their BET surface areas and in their volumes of the mesopores, as listed in Table 1. Their BET surface areas were in the range of 400–480 $m^2\ g^{-1}$ and increased with increasing Si/Al ratio.

The Si/Al ratio of the MOR zeolites definitely determines their acidic properties. Fig. 4 shows the TPD profiles of ammonia from the MOR zeolites with different Si/Al ratios. The *l*-peak attributed to the weak acid sites was observed at around 250 °C, while the *h*-peak attributed to the strong acid sites was observed at 400–450 °C [24,25]. The MOR(5) zeolite with the highest content of aluminum shows very large *l*- and *h*-peaks, indicating its high acid site density. The proportion of weak acid sites is small compared to that of strong acid sites. The increase in the Si/Al ratio of the MOR zeolites causes a significant decrease in both the *l*- and *h*-peaks. The small *h*-peak of the MOR(55) zeolite indicates the presence of only a small amount of strong acid sites. The MOR(103) zeolite has a very small amount of strong acid sites. The temperature at the maximum of the desorption peak shifts slightly towards a lower temperature with increasing Si/Al ratio of the MOR zeolites. This gradual shift of the maximum temperature may be due to the decrease in the acid site density, which lowers the readsorption of ammonia on the acid sites in the pores during its desorption [24]. The amount of acid sites on the MOR zeolites increases in the order of MOR(103) < MOR(55) < MOR(12) < MOR(5), as would be expected from the content of aluminum within them.

3.2. MTO reaction over the MOR zeolites

The conversion and product distribution of the MTO reaction over the MOR zeolites are quite dependent on the reaction conditions such as the temperature and the space velocity of methanol. In addition to the reaction conditions, the Si/Al ratio of the MOR zeolites is also an important factor in determining the conversion profiles over them, as shown in Fig. 5. All of the MOR zeolites, regardless of their Si/Al ratios, show high conversion at the initial time. However, the decrease in the conversion with the time on stream varies considerably with their Si/Al ratio. The conversion drops immediately on the MOR(5) zeolite with the highest acid site density: the conversion after 240 min is very low, about 20%. The conversion on the MOR(12) zeolite also decreases rapidly, but the decreasing rate over it is slower than that over the MOR(5) zeolite. However, the conversion over the MOR(55) and

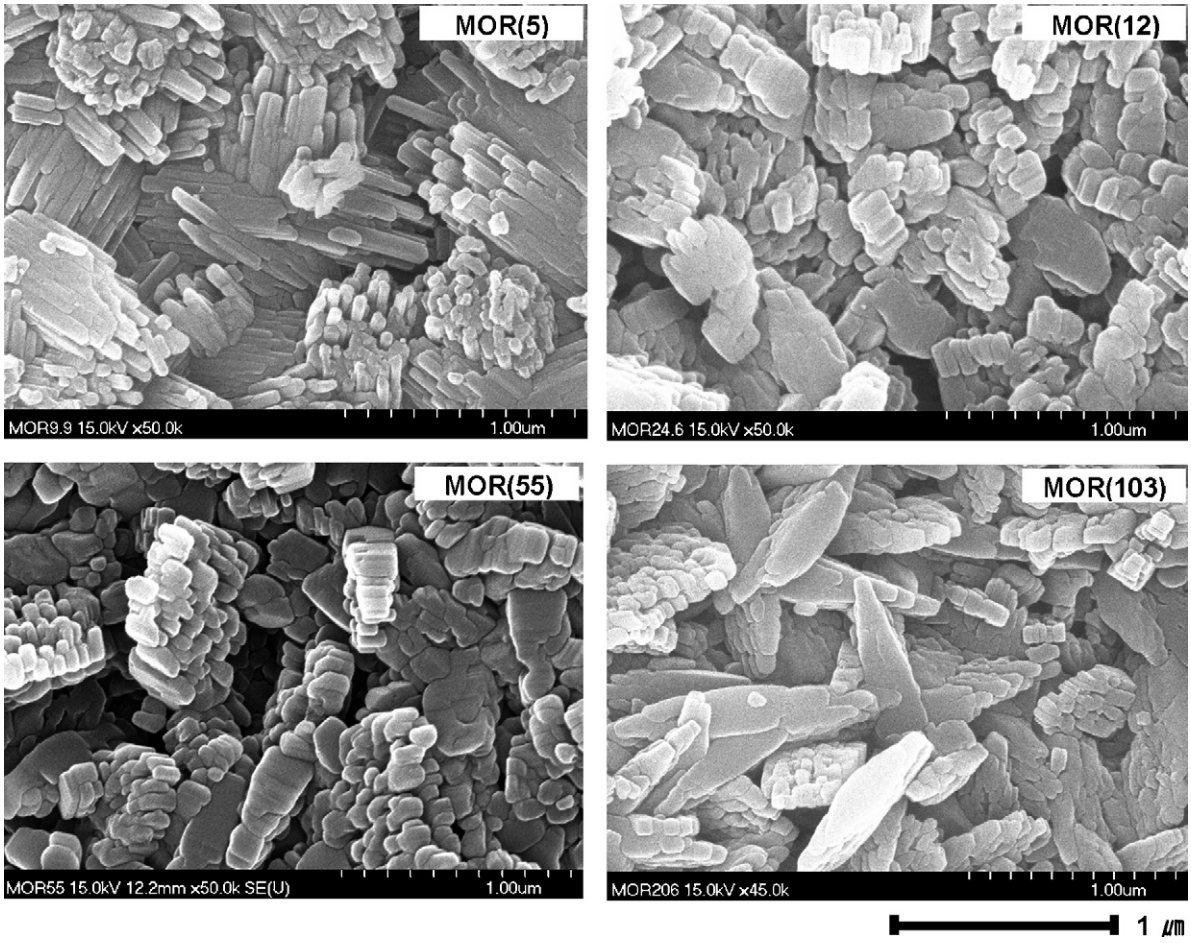

Fig. 2. SEM images of the MOR zeolites.

MOR(103) zeolites does not decrease for 240 min. The MOR zeolite with the highest acid site density deactivates rapidly, while that with the lowest acid site density maintains its activity under these reaction conditions.

The variation of the yield of the lower olefins with the time on stream over the MOR zeolites is also similar to that of the conversion (Fig. 6). At the initial time, the yield of the lower olefins over the MOR(5) zeolite was as high as 80%, while it rapidly decreased with the time on stream. Although the yield of the lower olefins over the MOR(12) zeolite decreases with the time on stream, the decreasing rate over it is slow compared to that over the MOR(5) zeolite. The yields of the lower olefins over the MOR(55) and MOR(103) zeolites remain at 65% under these reaction conditions, even after 240 min.

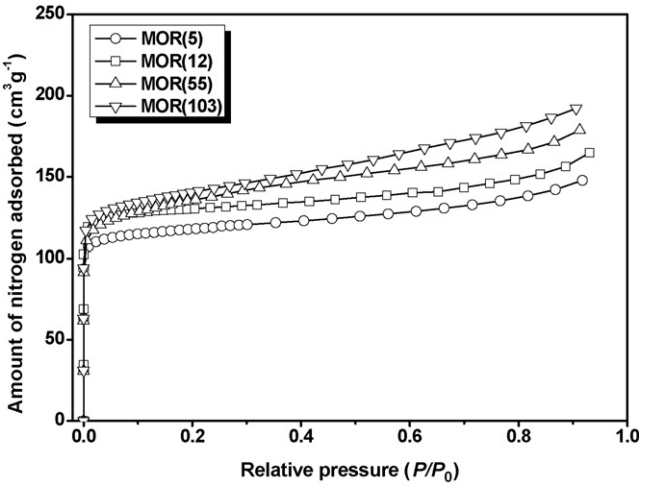

Fig. 3. N_2 adsorption isotherms of the MOR zeolites.

The composition of the lower olefins obtained over the MOR zeolites varies considerably with their Si/Al ratio. The yields of ethylene and propylene are high over the MOR(5) zeolite, while that of butenes is very low. On the contrary, the yields of propylene and butenes are high over the MOR(103) zeolite. The yield of butenes increases with increasing Si/Al ratio of the MOR zeolites, whereas that of ethylene decreases.

Table 2 compares the conversions and product compositions over the MOR zeolites after duration of the MTO reaction of 100 min. The conversion over the MOR(5) zeolite is low, 52.1%, due to its rapid deactivation. However, the conversions over the other MOR zeolites with higher Si/Al ratios are still above 90%, due to their slow deactivation. Ethylene, propylene and butenes are the major components, but the yield of each olefin varies with the Si/Al ratio of the MOR zeolites, as described above. The yields of ethylene over the MOR(5) and MOR(12) zeolites are high, while those over the MOR(55) and MOR(103) zeolites are low. The yields of propylene are high over the MOR(12), MOR(55) and MOR(103) zeolites. However, the yield of butene increases with increasing Si/Al ratio of the MOR zeolites. The yield of C_5^+ compounds including paraffins, alkylbenzenes and alkylnaphthalenes is as high as 35.5% on the MOR(55) zeolite.

Table 1
Pore characteristics and acidity of the MOR zeolites

Catalyst	Si/Al molar ratio[a]	S_{BET}[b] ($m^2\ g^{-1}$)	Pore volume ($cm^3\ g^{-1}$)		Desorbed amount of NH_3[e] (molecules g^{-1})	#Al content[f] (atom g^{-1})
			Micropore[c]	Mesopore[d]		
MOR(5)	5	400	0.14	0.06	8.6×10^{20}	6.2×10^{20}
MOR(13)	13	440	0.17	0.08	3.9×10^{20}	4.0×10^{20}
MOR(55)	55	465	0.15	0.12	0.9×10^{20}	0.8×10^{20}
MOR(103)	103	480	0.14	0.12	0.4×10^{20}	0.4×10^{20}

[a] Provided by the manufacturer.
[b] Calculated using BET equation.
[c] Calculated using *t*-plot method.
[d] Calculated using BJH method.
[e] Number of NH_3 atoms desorbed from the MOR zeolites.
[f] Calculated from the Si/Al molar ratio.

These product compositions can be summarized as follows: the yields of methane and ethylene are high on the partially deactivated MOR zeolites with a high acid site density. On the contrary, the fact that the yield of butenes is high on the MOR zeolites with a low acid site density indicates the preferable formation of butenes in their large pores. The continuous formation of alkylbenzenes and alkylnaphthalenes is also evident even over the MOR(103) zeolite with the lowest acid site density. While the small pore entrances of 8MR zeolites, such as SAPO-34 and LTA zeolites, limit the transfer of alkylbenzenes to the product stream in the MTO reaction over them [6], the large pores of the MOR zeolites allow the formation of alkylaromatics in the pores and transfer them out of the zeolites.

Fig. 7 compares the IR spectra of the materials occluded on the MOR(12) and MOR(103) zeolites in the MTO reaction at 350 °C for 10 min. Since the path of IR beam in the *in situ* cell is short, about 10 cm, and the concentrations of organic materials in the vapor phase are very low, the materials indicated by the differential IR spectra recorded during the MTO reaction correspond to those occluded on the zeolites. The IR spectra of MNP and TMB adsorbed on the MOR(12) zeolite at 120 °C are also shown in Fig. 7 for comparison.

These IR spectra can be divided into two parts, viz. the bands at 2700–3100 cm^{-1} attributed to the stretching vibration of the C–H bonds and the bands at 1300–1650 cm^{-1} attributed to the C=C and C–H bonds. Although the overall shapes of the IR spectra are very similar, each spectrum clearly shows certain specificities related to the acid site density. In the region of 1300–1650 cm^{-1} the materials occluded on the MOR(103) zeolite exhibit weak absorption bands composed of the nicely resolved bands at 1365, 1398, 1465, 1503 and 1599 cm^{-1}. On the contrary, the intensities of the absorption bands of the materials occluded on the MOR(12) zeolite are strong, but broad. These results mean that the amount of materials occluded on the MOR(12) zeolite is considerably larger than that on the MOR(103) zeolite. The large amount of materials with various configurations causes broad bands.

Table 3 lists the bands observed from the materials occluded on the MOR(103) and MOR(12) zeolites during the MTO reaction, along with their assignments deduced from previous reports and those from TMB and MNP adsorbed on the MOR(12) zeolite [26–36]. The absorption bands observed from TMB and MNP are also listed, in order to confirm the assignment of the bands. The IR spectrum recorded over the MOR(103) zeolite after a time on stream of 10 min shows seven small adsorption bands at 1365, 1398, 1465, 1503, 1599, 2857 and 2959 cm^{-1}. As listed in Table 3, the bands at 1365, 1398 and 1465 cm^{-1} are attributed to the bending vibration of the C–H bonds, and those at 1503 and 1599 cm^{-1} to the skeletal C=C vibration of aromatic compounds. The bands at 2857 and 2959 cm^{-1} are assigned to the stretching vibration of the C–H bonds in the methyl groups. These assignments strongly support the formation of alkylaromatics on the MOR(103) zeolite during the MTO reaction. Since the band at 1365 cm^{-1} is attributed to the isopropyl group substituted on the benzene ring, the alkylaromatics formed in the large pores of the MOR zeolites contain methyl, ethyl and isopropyl groups as substituents [26].

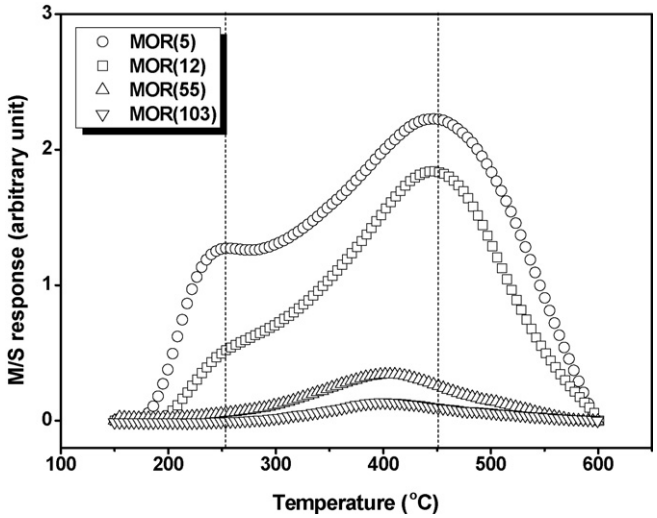

Fig. 4. TPD profiles of ammonia from the MOR zeolites.

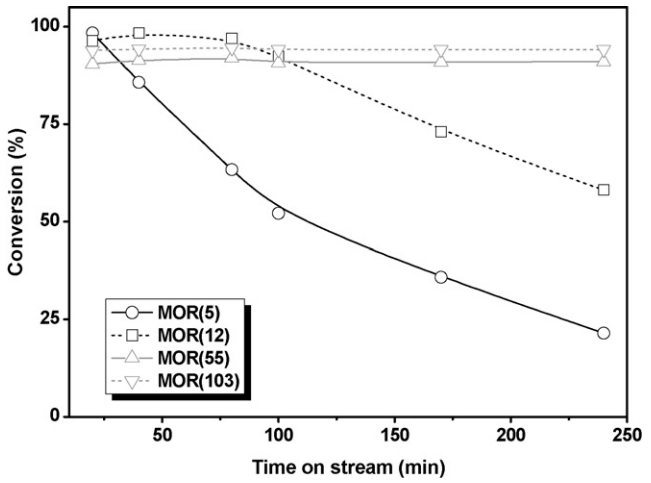

Fig. 5. Conversion profiles on the MOR zeolites in the MTO reaction: reaction temperature = 350 °C, WHSV = 0.70 h^{-1}.

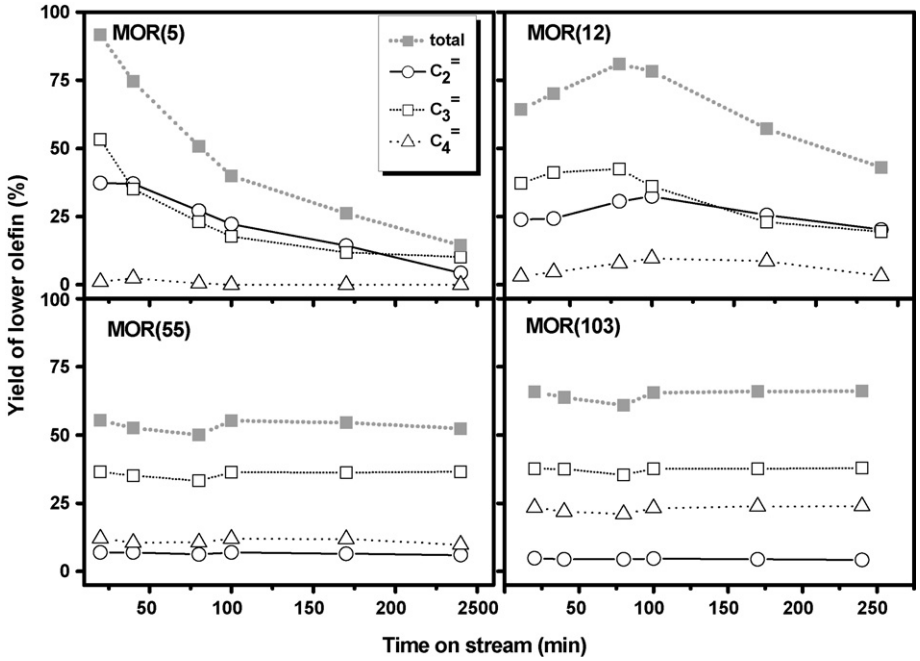

Fig. 6. Variation of the yield of lower olefins with the time on stream over the MOR zeolites in the MTO reaction: reaction temperature = 350 °C, WHSV = 0.70 h^{-1}.

Table 2
The product distribution in the MTO reaction over the MOR zeolites

Catalyst	Conversion (%)	Yield (%)						Aromatics[b]	
		C_1	$C_2^=$	$C_3^=$	C_4	$C_4^=$	C_5^+ [a]	Alkylbenzene	Alkylnaphthalene
MOR(5)	52.1	6.1	22.2	17.7	0.9	–	5.2	2.0	–
MOR(12)	92.4	2.1	32.4	36.1	5.4	9.7	6.7	2.1	0.5
MOR(55)	90.7	–	7.0	36.3	–	11.9	35.5	4.3	0.8
MOR(103)	94.1	–	4.7	37.6	–	23.2	28.6	3.8	2.3

Data reported at 100 min of time on stream. Reaction temperature = 350 °C, WHSV = 0.70 h^{-1}.
[a] Including C_5–C_{12} aliphatic and aromatics.
[b] Included in C_5^+.

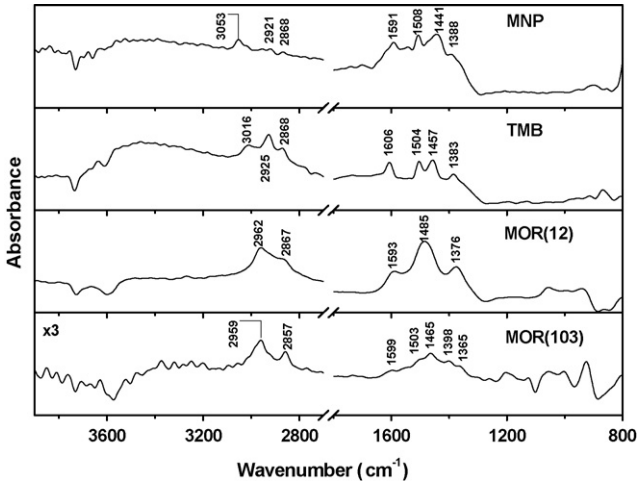

Fig. 7. *In situ* differential IR spectra of the materials occluded on the MOR(12) and MOR(103) zeolites during the MTO reaction at 350 °C for 10 min, WHSV = 0.70 h^{-1}. IR spectra of MNP and TMB adsorbed on the MOR(12) zeolite were also recorded at 120 °C for comparison.

On the contrary, the IR spectrum of the materials occluded on the MOR(12) zeolite in the frequency range of 1300–1600 cm^{-1} is slightly different from that of the materials occluded on the MOR(103) zeolite. The large amounts of occluded materials cause the overlapping of the bands, resulting in three bands at 1376, 1485 and 1593 cm^{-1}. The overlapping of the bending vibration of the C–H bond and skeletal vibration of the aromatic rings leads to the band at 1485 cm^{-1}. However, the new band at 1593 cm^{-1} is attributed to the skeletal vibration of the C=C bond of PAH occluded in the pores. The broadness of the band at around 1600 cm^{-1} renders the confirmation of the presence of carbenium ions on the MOR zeolites difficult [33,37].

For the more careful assignment of the band at 1500–1600 cm^{-1}, Fig. 8 shows the IR spectra of the materials occluded on the MOR(12) and MOR(103) zeolites recorded *in situ* during the MTO reaction of deuterium enriched methanol, CD_3OD. Since the C–D and O–D bands are observed at different wavenumbers from those of C–H and O–H, respectively, it is possible to clearly assign the IR bands of the C–H bond of the methyl group and C=C bonds of the aromatic rings.

The bands at 3585, 3690 and 3733 cm^{-1} attributed to the O–H bands on the MOR(103) zeolite disappeared in the MTO reaction of CD_3OD, while new bands appeared at 2652, 2704 and 2748 cm^{-1} due to the formation of O–D groups. The bands at 2079 and 2225 cm^{-1} represent the C–D bonds of the deuterium enriched

Table 3
Vibrational frequencies of the materials occluded on the MOR(103) and MOR(12) zeolites and MNP and TMB adsorbed on the MOR(12) zeolite [26–36]

Band (cm^{-1})	Assignment	MOR(103)[a]	MOR(12)[a]	TMP[b]	MNP[b]	Reference
1366	CH_3 deformation (attached to isopropylbenzene)	1365	1376	–	–	[26]
1385–1393	Aromatic–polyaromatics/$\delta_s CH_3$	1398	–	1383	1388	[27,28]
1437–1463	Aromatic–polyaromatics/$\delta_{as} CH_3$	1465	1485	1457	1441	[29]
1471	CH_2 deformation (attached to aromatic)/$\delta_{as} CH_3$ from methanol			–	–	[30]
1513/1524	γC=C aromatics	1503	–	1504	1508	[31,32]
1589/1595	γC=C aromatics/polycyclic aromatics	1599	1593	–	1591	[31]
1604	γC=C aromatics of carbenium ion		–	1606	–	[33]
2865/2855	$\gamma_a CH_3$ saturated CH/$\gamma_a CH_3$ from methanol	2857	2867	2868	2868	[30,34,35]
2925–2936	$\gamma_a CH_2$ saturated CH/overtone of $\delta_{as} CH_3$ attached to aromatic	–	–	2925	2921	[34,36]
2960/2958	$\gamma_{as} CH_3$ saturated CH/$\gamma_{as} CH_3$ from methanol	2959	2962	–	–	[30,34,35]
3045/3058	γCH aromatic	–	–	3016	3019/3053	[31]

[a] Adsorbed or occluded materials on the MOR zeolites in MTO reaction at 350 °C.
[b] Adsorbed on the MOR(12) zeolite at 120 °C.

methyl group [38–42]. The strong absorption due to the skeletal Si–O vibration interferes with the observation of the bending vibration of C–D at 1000–1100 cm^{-1}. The bands at 1465 and 1570 cm^{-1} are commonly observed in the IR spectra of the materials occluded on the MOR zeolites in the MTO reaction of both CH_3OH and CD_3OD, irrespective of the deuterium enrichment. This means that these bands should be attributed to the skeletal C=C bonds of aromatic rings, not to the bending vibration of C–H bonds. The band observed at 1465 cm^{-1} increased rapidly on both the MOR(12) and MOR(103) zeolites at the initial time. However, the band at 1570 cm^{-1} is small at the initial time and steadily increases with increasing time on stream. Therefore, the band at 1465 cm^{-1} can be attributed to the skeletal C=C bond of the reaction intermediates including HMB, while the steady increase in the band at 1570 cm^{-1} indicates that it is related to the skeletal C=C bond of the PAHs occluded on the MOR zeolite in the MTO reaction.

The acid site density of the MOR zeolites is responsible for the intensity and increasing rate of the bands at both 1465 and 1570 cm^{-1}. Fig. 9 shows the changes of the bands at 1465 and 1570 cm^{-1} observed on the MOR zeolites with the time on stream of the MTO reaction. The intensity of the band at 1465 cm^{-1} increases rapidly at the initial time, regardless of the Si/Al ratio, even through its height varies considerably with the acid site density. The similarity of these trends over all of the MOR zeolites strongly suggests that the band at 1465 cm^{-1} is responsible for the reactive intermediates. The MOR(5) zeolite with the highest acid site density has a lot of intermediates, while the MOR(103) zeolite has only a small amount. On the other hand, the band at 1570 cm^{-1} increases steadily with increasing time on stream over all of the MOR zeolites. The steady increase of the band at 1570 cm^{-1} up to very high absorbance over the MOR(5) zeolite indicates the large accumulation of PAH on its pores. The low intensities of the bands at 1570 cm^{-1} over the MOR(55) and MOR(103) zeolites indicate that small amounts of PAH are occluded on them.

The ^{13}C MAS NMR spectra of the materials occluded on the MOR(5) and MOR(103) zeolites also confirm the formation of alkylaromatics in their pores, as shown in Fig. 10. The peaks at 10–35 ppm are attributed to the carbon atoms of alkyl groups and those at 120–150 ppm to the carbon atoms of aromatic rings. Therefore, these spectra definitely suggest the occlusion of alkylaromatics on the MOR zeolites during the MTO reaction [43–45]. These spectra are very similar to each other, except for the strong peak at 49.2 ppm for the materials occluded on the MOR(103) zeolite. The other difference is the broadness of the peaks of the materials occluded on the MOR(5) zeolite compared to those on the MOR(103) zeolite. The broad and large peaks at 120–150 ppm of the materials occluded on the MOR(5) zeolite indicate the presence of various PAHs in its pores. On the contrary, the sharp peaks at 16.3 and 132.8 ppm, which are the characteristic peaks of HMB, indicate that the major component of the materials occluded on the MOR(103) zeolite is HMB [43]. The presence of the sharp

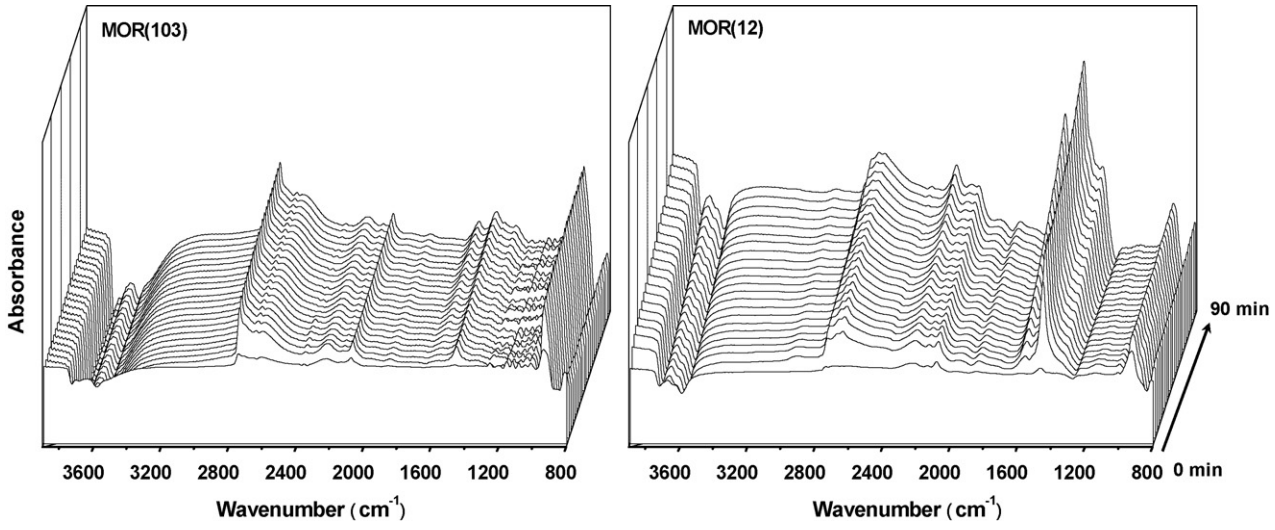

Fig. 8. *In situ* differential IR spectra of the materials occluded on the MOR(103) and MOR(12) zeolites during the MTO reaction of CD_3OD for 4–90 min: reaction temperature = 350 °C, WHSV = 0.70 h^{-1}.

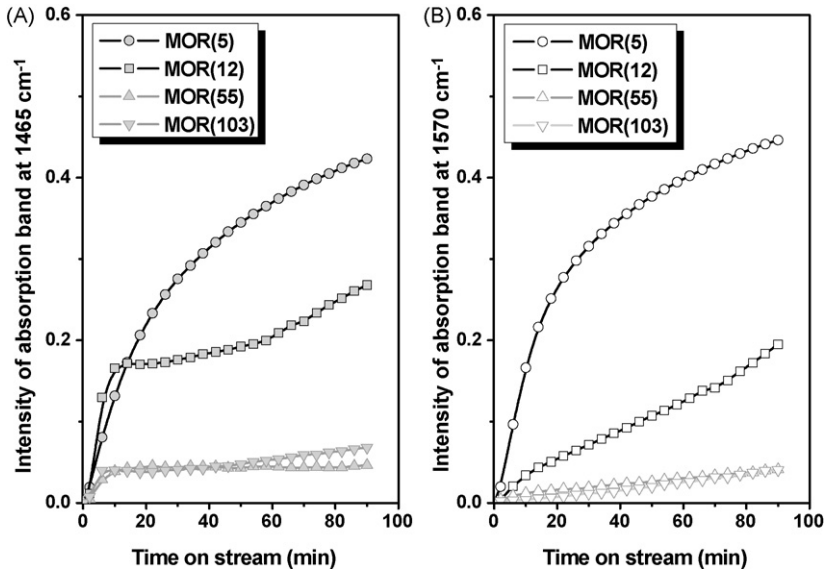

Fig. 9. The changes in the intensities of 1465 cm^{-1} (A) and 1570 cm^{-1} (B) with the time on stream over the MOR zeolites during the MTO reaction of CD_3OD: reaction temperature = 350 °C, WHSV = 0.70 h^{-1}.

peak at 49.2 ppm, which is related to methanol adsorbed on the acidic zeolites, suggests that the MOR(103) zeolite is still active as a catalyst for the MTO reaction [43,45].

The thermogravimetric analysis of the MOR zeolites used in the MTO reaction indicates a considerable variance of the amount of organic materials occluded on them. The TGA thermograms (not shown) of the used MOR zeolites recorded in air provide information on the amount of PAH or carbon deposited on them. The weight losses in the used MOR(5) and MOR(12) zeolites related to the organic materials are as large as 12.4 and 12.1%, respectively. However, the weight losses in the used MOR(55) and MOR(103) zeolites are small, being in the range of 0.5–0.7%. Large amounts of organic materials with high boiling points are formed and occluded on the MOR zeolites with a high acid site density, while the amounts of materials occluded on the MOR zeolite with a low acid site density are small.

Fig. 11 shows the UV–vis spectra of the organic materials extracted from the MOR zeolites used in the MTO reaction. The absorption ranges of the extracts vary considerably according to their Si/Al ratio. The extract from the used MOR(5) zeolite shows a large and broad absorption band in the range of 250–500 nm. The absorbance is still high, 0.2, even at 450 nm. The absorption range of the extract from the used MOR(12) zeolite is also wide, 250–450 nm. On the contrary, the extracts from the used MOR(55) and MOR(103) zeolites show relatively small and narrow absorption bands of 250–350 nm. The difference in the UV–vis spectra of these extracts indicates that the species of the materials occluded on the MOR zeolites are all alkylaromatics, but that the number of fused rings varies according to their acid site density.

The maximum wavelength of the UV–vis absorption of methylbenzenes including HMB is observed at 260 nm, while that of PAH with large numbers of fused aromatic rings is observed at higher wavelengths [44]. Naphthalene shows a maximum wavelength at 270 nm, anthracene at 350 nm and pyrene at 390 nm. The fact that the extracts from the used MOR(5) and MOR(12) zeolites have intense and broad absorption bands in the range of 250–500 nm indicates the occlusion of PAH with large numbers of fused rings in their pores. Furthermore, the strong absorption bands are indicative of a large amount of occluded materials. On the other hand, the narrow and weak bands in the

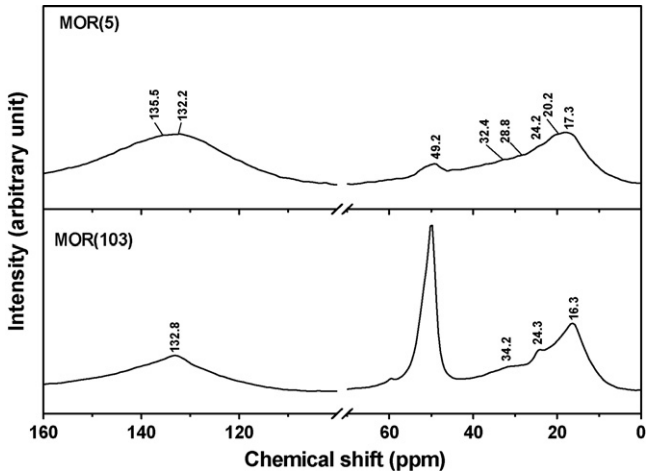

Fig. 10. *Ex situ* ^{13}C MAS NMR spectra of materials adsorbed and occluded on the MOR zeolites during the MTO reaction for 90 min: reaction temperature = 350 °C, WHSV = 0.70 h^{-1}.

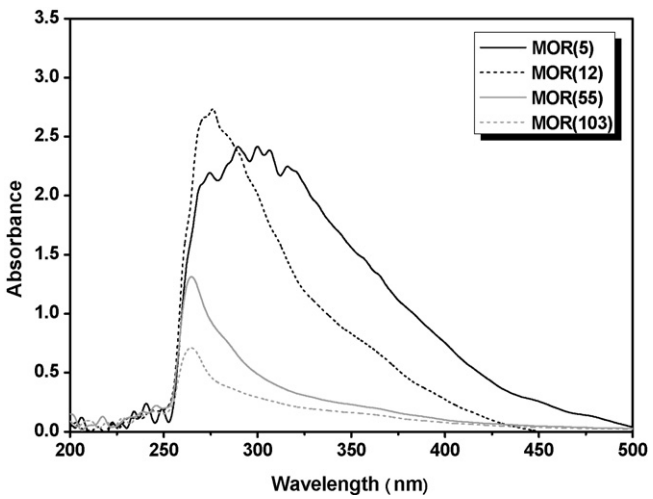

Fig. 11. UV–vis spectra of occluded materials on the MOR zeolites in the MTO reaction for 240 min: reaction temperature = 350 °C, WHSV = 0.70 h^{-1}.

range of 250–300 nm for the extracts from the used MOR(55) and MOR(103) zeolites is due to the small amount of occluded materials composed of alkylbenzenes and alkylnaphthalenes that include of 1–2 fused rings. The extract from the used MOR(103) zeolite also shows an appreciable absorption at 350 nm, indicating the formation of anthracene derivatives in its pores, even though their contents are very low.

4. Discussion

Since the MOR zeolites with different Si/Al ratios used in this study show no meaningful differences in their XRD patterns, SEM photos and N_2 adsorption isotherms, the contribution of their physical properties, based on their framework and pore structures, to their catalytic properties, except for the acid site density, can be neglected. The dealumination of the parent MOR zeolite to prepare the MOR zeolites with higher Si/Al ratios removes its amorphous materials as well as aluminum atoms from its framework, thereby increasing slightly the diffraction peaks and BET surface areas of the latter [46].

The acidic properties of the MOR zeolites vary significantly with their Si/Al ratios. The large *h*-peak of the MOR(5) zeolite with a low Si/Al ratio indicates the presence of a large amount of strong acid sites on it, as shown in Fig. 4. On the contrary, the MOR(103) zeolite with a high Si/Al ratio shows a small *h*-peak, indicating that it has a small amount of strong acid sites. The amounts of ammonia molecules desorbed from the MOR zeolites are in good agreement with the amounts of aluminum atoms contained within them, as listed in Table 1. This means that most of the aluminum atoms contained in the MOR zeolites participate in the formation of acid sites and, thus, the co-existence of non-framework aluminum is negligible. In addition, the number of acid sites on the MOR(5) zeolite is 20 times larger than that on the MOR(103) zeolite, which is sufficient to examine the effect of the acid site density on the product selectivity and deactivation of the MOR zeolite in the MTO reaction.

The MOR zeolites, regardless of their Si/Al ratios, show a high conversion and high yield of the lower olefins at the initial time. However, the deactivation rate of the MOR zeolites varies considerably with their acid site density as deduced from their Si/Al ratios. The MOR(5) and MOR(12) zeolites with a high acid site density show rapid deactivation. However, the deactivation rates over the MOR(55) and MOR(103) zeolites are slow, due to their low acid site density. This means that the acid site density of the MOR zeolites determines their deactivation rate in the MTO reaction. The variation of the yield of the lower olefins with the time on stream shows similar behavior to that of the conversion. As a result, the product yields over the MOR zeolites also vary according to their acid site density.

The product composition of the MTO reaction over the MOR zeolites varies with their acid site density. As shown in Table 2, the yield of ethylene over the MOR(5) zeolite was high, but that of alkylaromatics was low. On the other hand, the yields of propylene and butenes are high over the MOR(55) and MOR(103) zeolites. The yield of alkylaromatics was also high on these zeolites. Since the 12MR pores of the MOR zeolites are large, about 0.7 nm in diameter, there is no limitation in the formation of paraffin, olefin and even alkylaromatics in the product streams of the MTO reaction. Therefore, the difference in the product composition of the MTO reaction over the MOR zeolites according to their acid site density is due to the extent of the reaction carried out in their pores.

Since the conversion level over the MOR(103) zeolite still remains above 90% even after 100 min of reaction time, the product distribution that is obtained reflects the MTO reaction over the MOR zeolite in the fresh state. The high yields of propylene and butenes over the MOR(103) zeolite with the lowest acid site density indicate that these olefins may be the primary olefins. The high yield of C_5^+ containing alkylaromatics reflects the formation of large aromatic molecules in the pores of the MOR zeolite. Kolboe and co-workers suggested the heptamethylbenzene carbenium ion as the active intermediate in the MTO reaction over beta zeolite [47], while HMB is a well-known intermediate of the MTO reaction over the SAPO-34 molecular sieve. If the MTO reactions over the MOR zeolites also proceed through methylbenzenes, following the hydrocarbon pool mechanism, as in the case of beta zeolite and the SAPO-34 molecular sieve, the large pores of the MOR zeolite would allow the formation of alkylaromatics, with larger alkyl groups such as isopropyl and butyl groups, as substituents. Therefore, the high yields of propylene and butane over the MOR(103) zeolite are due to the large pores of the MOR zeolites allowing the formation of alkylaromatic intermediates with large alkyl substitutions. The large pores also allow the transfer of methylbenzenes and methylnaphthalenes to the product stream, resulting in a higher C_5^+ yield including alkylaromatics. On the contrary, the yields of methane and ethylene are high over the deactivated MOR(5) zeolite. Methane cannot be formed directly from methylbenzene through a paring or side-chain alkylation reaction. Therefore, it is produced from either the secondary products of the oligomerization cracking of the lower olefins or the cracking products of PAH.

The amounts and species of the materials occluded on the MOR zeolites in the MTO reaction vary considerably according to their acid site density. The rapid formation of PAH over the MOR(5) zeolite with the highest acid site density was evident from its IR and ^{13}C NMR spectra. The high absorbance at 250–500 nm of the extract obtained from it indicates the occlusion of PAH composed of 3–4 fused benzene rings in its pores. The high concentration of alkylaromatics in the pores of the MOR(5) and MOR(12) zeolites induces the formation of large PAH molecules with a large number of fused rings. Since large PAH molecules with a high boiling point are easily occluded on the pores of the MOR zeolite, the accumulation of PAHs is responsible for its rapid deactivation. On the contrary, alkylbenzenes and alkylnaphthalenes without large fused benzene rings are formed in the MOR(103) zeolite with the lowest acid site density. The low acid site density of the MOR(55) and MOR(103) zeolites results in their having a long catalyst life with slow deactivation.

MOR zeolites with large 12MR linear pores are also active in the MTO reaction, as in the case of the SAPO-34 molecular sieve with 8MR pore entrances, but the selectivity for the lower olefins over the former is low compared to that over the latter. The relatively high selectivities for butenes and C_5^+ on the MOR zeolites, regardless of their acid site density, are due to the formation of alkylaromatics with large alkyl substituents in their large pores.

5. Conclusions

MOR zeolites, regardless of their acid site density, are highly active and selective for the lower olefins at the initial time. However, their deactivation rates vary considerably according to their acid site density. The MOR(5) zeolite with the highest acid site density deactivates rapidly with increasing time on stream, while the MOR(103) zeolite with the lowest acid site density retains its activity even after 240 min under these reaction conditions. Alkylaromatics are commonly produced in the pores of the MOR zeolites in the MTO reaction, but the acid site density of the MOR zeolites determines their rate of condensation to PAH. The MOR zeolites with a high acid site density prefer to form PAH with a large number of fused rings, resulting in their rapid deactivation. The MOR zeolites with a low acid site density induce the sparse distribution of alkylaromatics in

the pores, suppressing the condensation to PAH. The low acid site density of the MOR zeolites is responsible for their slow deactivation, allowing them to sustain their catalytic activity, thus producing lower olefins. The low selectivity for the ethylene and propylene of the MOR zeolites compared to the SAPO-34 molecular sieve is inevitable, because their large 12MR pores allow the formation of alkylaromatic intermediates with large alkyl substituents which can produce C_4–C_5 olefins.

Acknowledgement

The authors would like to acknowledge the funding from the Korea Ministry of Commerce, Industry and Energy (MOCIE) through the "Project of next-generation novel technology development" of ITEP.

References

[1] M. Stocker, Micropor. Mesopor. Mater. 29 (1999) 3–48.
[2] F.J. Keil, Micropor. Mesopor. Mater. 29 (1999) 49–66.
[3] S.M. Abubakar, D.M. Marcus, J.C. Lee, J.O. Ehresmann, C.-Y. Chen, P.W. Kletnieks, D.R. Guenther, M.J. Hayman, M. Pavlova, J.B. Nicholas, J.F. Haw, Langmuir 22 (2006) 4846–4852.
[4] S. Wilson, P. Barger, Micropor. Mesopor. Mater. 29 (1999) 117–126.
[5] J.Q. Chen, A. Bozzano, B. Glover, T. Fuglerud, S. Kvisle, Catal. Today 106 (2005) 103–107.
[6] J.W. Park, J.Y. Lee, K.S. Kim, S.B. Hong, G. Seo, Appl. Catal. A: Gen. 339 (2008) 36–44.
[7] A.J. Marchi, G.F. Froment, Appl. Catal. A: Gen. 94 (1993) 91–106.
[8] Ø. Mikkelsen, S. Kolboe, Micropor. Mesopor. Mater. 29 (1999) 173–184.
[9] M.A. Aramendia, V. Borau, C. Jimenez, J.M. Marinas, R. Roldan, F.J. Romero, F.J. Urbano, Chem. Lett. (2002) 672–673.
[10] M. Sawa, M. Niwa, Y. Murakami, Chem. Lett. (1987) 1637–1640.
[11] M. Bjorgen, S. Kolboe, Appl. Catal. A: Gen. 225 (2002) 285–290.
[12] C.D. Chang, Catal. Rev. Sci. Eng. 25 (1) (1983) 1–118.
[13] J.F. Haw, W. Song, D.M. Marcus, J.B. Nicholas, Acc. Chem. Res. 36 (2003) 317–326.
[14] W. Song, H. Fu, J.F. Haw, J. Am. Chem. Soc. 123 (2001) 4749–4754.
[15] W. Song, J.F. Haw, J.B. Nicholas, C.S. Heneghan, J. Am. Chem. Soc. 122 (2000) 10726–10727.
[16] H. Fu, W. Song, J.F. Haw, Catal. Lett. 76 (1–2) (2001) 89–94.
[17] J.F. Haw, D.M. Marcus, Top. Catal. 34 (2005) 41–48.
[18] J.-H. Kim, Y. Sugi, T. Matsuzaki, T. Hanaoka, Y. Kubota, X. Tu, M. Matsumoto, Micropor. Mater. 5 (1995) 113–121.
[19] Y. Sugi, S. Tawada, T. Sugimura, Y. Kubota, T. Hanaoka, T. Matsuzaki, K. Nakajima, Appl. Catal. A: Gen. 189 (1999) 251–261.
[20] J.S. Jung, J.W. Park, G. Seo, Appl. Catal. A: Gen. 288 (2005) 149–157.
[21] Y. Sugi, H. Maekawa, S.A.R. Mulla, A. Ito, C. Naitoh, K. Nakagawa, K. Komura, Y. Kubota, J.-H. Kim, G. Seo, Bull. Chem. Soc. Jpn. 80 (2007) 1418–1428.
[22] M.M.J. Treacy, J.B. Higgins, Collection of Simulated XRD Powder Patterns for Zeolites, 5th ed., Elsevier, New York, 2007.
[23] G.J. Kim, W.S. Ahn, Zeolites 11 (1991) 745–750.
[24] N. Katada, H. Igi, J.-H. Kim, M. Niwa, J. Phys. Chem. B 101 (1997) 5969–5977.
[25] M. Niwa, N. Katada, M. Sawa, Y. Murakami, J. Phys. Chem. 99 (21) (1995) 8812–8816.
[26] M. Hunger, Micropor. Mesopor. Mater. 82 (2005) 241–255.
[27] J. Pater, F. Cardona, C. Canaff, N.S. Gnep, G. Szabo, M. Guisnet, Ind. Eng. Chem. Res. 38 (1999) 3822–3829.
[28] C. Li, P.C. Stair, Catal. Today 33 (1997) 353–360.
[29] L.M. Petkovic, D.M. Ginosar, K.C. Burch, J. Catal. 234 (2005) 328–339.
[30] T.R. Forester, R.F. Howe, J. Am. Chem. Soc. 109 (1987) 5076–5082.
[31] P. Andy, N.S. Gnep, M. Guisnet, E. Benazzi, C. Traversy, J. Catal. 173 (1998) 322–332.
[32] H.G. Karge, W. NieBen, H. Bludau, Appl. Catal. A: Gen. 146 (1996) 339–349.
[33] M. Bjørgen, F. Bonino, B. Arstad, S. Kolboe, K.-P. Lillerud, A. Zecchina, S. Bordiga, ChemPhysChem 6 (2005) 232–235.
[34] X. Lin, Y. Fan, G. Shi, H. Liu, X. Bao, Energy Fuels 21 (2007) 2517–2524.
[35] Q. Zhu, J.N. Kondo, T. Tatsumi, S. Inagaki, R. Ohnuma, Y. Kubota, Y. Shimodaira, H. Kobayashi, K. Domen, J. Phys. Chem. C 111 (2007) 5409–5415.
[36] M. Trombetta, G. Busca, S. Rossini, V. Piccoli, U. Cornaroy, J. Catal. 168 (1997) 349–363.
[37] M. Bjørgen, F. Bonino, S. Kolboe, K.-P. Lillerud, A. Zecchina, S. Bordiga, J. Am. Chem. Soc. 125 (2003) 15863–15868.
[38] F. Ouyang, J.N. Kondo, K. Maruya, K. Domen, J. Chem. Soc., Faraday Trans. 93 (1) (1997) 169–174.
[39] E. Yoda, J.N. Kondo, F. Wakabayashi, K. Domen, Appl. Catal. A: Gen. 194–195 (2000) 275–283.
[40] J.N. Kondo, F. Wakabayashi, K. Domen, Catal. Lett. 53 (1998) 215–220.
[41] J.N. Kondo, L. Shao, F. Wakabayashi, K. Domen, J. Phys. Chem. B 101 (1997) 9314–9320.
[42] J. Rakoczy, Zeolites 13 (1993) 256–260.
[43] http://riodb01.ibase.aist.go.jp/sdbs/cgi-bin/direct_frame_top.cgi, Spectral Database for Organic Compounds (SDBS).
[44] W. Simon, J. Seibl, T. Clerc, K. Biemann, in: W. Fresenius, J.F.K. Huber, E. Pungor, G.A. Rechnitz, W. Simon, Th.S. West (Eds.), Tables of Spectral Data for Structure Determination of Organic Compounds, 2nd ed., Springer-Verlag, New York, 1989.
[45] Y. Jiang, J. Huang, V.R. Reddy Marthala, Y.S. Ooi, J. Weitkamp, M. Hunger, Micropor. Mesopor. Mater. 105 (2007) 132–139.
[46] M. Boveri, C. Marquez-Alvarez, M.A. Laborde, E. Sastre, Catal. Today 114 (2006) 217–225.
[47] M. Bjørgen, U. Olsbye, S. Svelle, S. Kolboe, Catal. Lett. 93 (1–2) (2004) 37–40.